

On the origin of rR_1 ring structures in barred galaxies

M. Romero-Gómez^{1,3}, J.J. Masdemont², E. Athanassoula³, and C. García-Gómez¹

¹ D.E.I.M., Universitat Rovira i Virgili, Campus Sescelades, Avd. dels Països Catalans 26, 43007 Tarragona, Spain

² I.E.E.C & Dep. Mat. Aplicada I, Universitat Politècnica de Catalunya, Diagonal 647, 08028 Barcelona, Spain

³ LAM, Observatoire Astronomique de Marseille Provence, 2 Place Le Verrier, 13248 Marseille Cédex 04, France

Received 15 August

Abstract. We propose a new theory for the formation of rR_1 ring structures, i.e. for ring structures with both an inner and an outer ring, the latter having the form of “8”. We propose that these rings are formed by material from the stable and unstable invariant manifolds associated with the Lyapunov orbits around the equilibrium points of a barred galaxy. We discuss the shape and velocity structure of the rings thus formed and argue that they are in agreement with the observed properties of rR_1 structures.

Key words. galaxies – structure – ringed galaxies

1. Introduction

Barred galaxies often show spectacular rings whose different types have been classified by Buta (1986a) as follows: Nuclear rings (which are not discussed here) which surround the nucleus and that are much smaller in size than the bar. At larger radii there are inner rings, denoted in Buta’s (1986a) classification by a “ r ”, which surround the bar and which have the same size and orientation as the bar. And there are outer rings, denoted by R , which are bigger than the bar. These “pure” rings are defined to be distinct and closed, but one can often find unclosed or partial ring patterns of spiral character, and these are referred to as “pseudorings” and denoted R' . A particular class of outer rings called R_1 or R_1' , for pseudorings, has two main arms forming an eight-shaped ring or pseudoring, with its major axis perpendicular to the bar. NGC 1326 is a well studied example of an $(R_1)SB(r)0/a$ galaxy (Buta 1995). Its bar is surrounded by an inner ring which is almost exactly aligned with the bar and has roughly the same diameter. Its outer ring is clearly R_1 and is elongated perpendicular to the bar (Buta et al. 1998, see Fig. 1).

Schwarz (1981, 1984, 1985) showed that ring-like structures can arise around the Lindblad resonances due to a bar-like perturbation of the galaxy potential. The gas will be forced to rearrange its distribution and generate a spiral. Near the outer Lindblad resonances the crossing of perturbed trajectories will develop a ring-like pattern. In these regions, gas clouds will collide and will form spiral shock fronts which will slowly change as a result of torques exerted by the bar and evolve into



Fig. 1. Image of the rR_1 galaxy NGC 1326 showing a well developed $(R_1)SB(r)0/a$ structure. (Digital Sky Survey ©Anglo Australian Observatory Board)

a ring structure which, after star formation, will be populated by stars in near-resonant periodic orbits.

Danby (1965) argued that orbits in the gravitational potential of a bar play an important role in the formation of arms. He noted that orbits departing from the vicinity of the equilibrium points located at the ends of the bar describe loci with the shape of spiral arms and can be responsible for transport of stars from within to outside corotation, and viceversa. Unfortunately, he did not set his work in a rigorous theoretical context, so

that it remained purely phenomenological. He also investigated whether orbits can be responsible for ring-like structures, but, in this case, he did not consider orbits departing from the ends of the bar as he previously did when accounting for the spiral arms. He concluded that rings would require high energy orbits, while we will see in this paper that mainly low energy orbits can constitute the rings.

Here we propose a new dynamical model, applicable to the particular case of rR_1 class of ringed galaxies. We expect that more detailed modelling will extend this new model to the rest of the ringed galaxy classes. The model is based on the orbital motion of stars in the vicinity of equilibrium points in the rotating bar potential and does not rely on additional star formation. The tools we use in our model are well known in celestial mechanics but have not been much used so far in galactic dynamics. We therefore start, in section 2, by introducing the equations of motion and the equilibrium points. In section 3 we describe the dynamics around the Lagrangian point L_1 and we introduce the invariant manifolds. We discuss the linear case in subsection 3.1 and the general case in subsection 3.2. In section 4 we describe the role of the invariant manifolds in the transport of stars and their properties in the framework of ringed barred galaxies. In section 5 we describe briefly how invariant manifolds are computed numerically and we apply them to a specific model. Finally, section 6 discusses the properties of the spiral arms thus produced and summarises our results.

2. Equations of motion and equilibrium points

We model the potential of the galaxy as the superposition of two components, one axisymmetric and the other barlike. The latter rotates clockwise at angular velocity $\mathbf{\Omega}_p = \Omega_p \mathbf{e}_z$, where $\Omega_p > 0$ is the pattern speed considered here to be constant¹. The equations of motion in the frame rotating with $\mathbf{\Omega}_p$ are:

$$\ddot{\mathbf{r}} = -\nabla\Phi - 2(\mathbf{\Omega}_p \times \dot{\mathbf{r}}) - \mathbf{\Omega}_p \times (\mathbf{\Omega}_p \times \mathbf{r}), \quad (1)$$

where the terms $-2\mathbf{\Omega}_p \times \dot{\mathbf{r}}$ and $-\mathbf{\Omega}_p \times (\mathbf{\Omega}_p \times \mathbf{r})$ represent the Coriolis and the centrifugal forces, respectively, and \mathbf{r} is the position vector.

Following Binney & Tremaine (1987), we take the dot product of equation (1) with $\dot{\mathbf{r}}$, and rearranging the resulting equation, we obtain

$$\frac{dE_J}{dt} = 0,$$

where

$$E_J \equiv \frac{1}{2} |\dot{\mathbf{r}}|^2 + \Phi - \frac{1}{2} |\mathbf{\Omega}_p \times \mathbf{r}|^2.$$

E_J is known as the Jacobi integral or Jacobi constant. Notice that this is the sum of $\frac{1}{2} \dot{\mathbf{r}}^2 + \Phi$, which is the energy in a nonrotating frame, and of the quantity $-\frac{1}{2} |\mathbf{\Omega}_p \times \mathbf{r}|^2 = -\frac{1}{2} \Omega_p^2 (x^2 + y^2)$, which can be thought of as the “potential energy” to which the centrifugal “force” gives rise. So if we define an effective potential

$$\Phi_{\text{eff}} = \Phi - \frac{1}{2} \Omega_p^2 (x^2 + y^2),$$

¹ Bold letters denote vector notation.

equation (1) becomes

$$\ddot{\mathbf{r}} = -\nabla\Phi_{\text{eff}} - 2(\mathbf{\Omega}_p \times \dot{\mathbf{r}}), \quad (2)$$

and the Jacobi constant is

$$E_J = \frac{1}{2} |\dot{\mathbf{r}}|^2 + \Phi_{\text{eff}},$$

so that it can be considered as the “energy” in the rotating frame.

The surface $\Phi_{\text{eff}} = E_J$ is called the zero velocity surface and its cut with the $z = 0$ plane is the zero velocity curve. All regions in which $\Phi_{\text{eff}} > E_J$ are forbidden to a star and we call them forbidden regions. Fig. 2b shows an example of zero velocity curves and the regions delimited by them, namely the exterior, interior and forbidden regions, for the potential introduced in section 5.

Φ_{eff} has five equilibrium points, named L_1 to L_5 , located in the xy plane, at which $\frac{\partial\Phi_{\text{eff}}}{\partial x} = \frac{\partial\Phi_{\text{eff}}}{\partial y} = \frac{\partial\Phi_{\text{eff}}}{\partial z} = 0$. Due to their similarity to the corresponding points in the restricted three body problem, they are often called Lagrangian points. L_1 and L_2 lie on the x -axis and are symmetric with respect to the origin. L_3 lies on the origin of coordinates. Finally, L_4 and L_5 lie on the y -axis and are also symmetric with respect to the origin (see Fig.2a, again for the potential introduced in section 5).

We can check the stability of the Lagrangian points by considering the motion in their immediate neighbourhood². If we expand Φ_{eff} around one of these points and retain only first order terms, the equations of motion (2) become

$$\begin{cases} \ddot{x} = 2\Omega_p \dot{y} - \Phi_{xx} x \\ \ddot{y} = -2\Omega_p \dot{x} - \Phi_{yy} y \\ \ddot{z} = -\Phi_{zz} z \end{cases} \quad (3)$$

where we have defined

$$x \equiv x - x_L; \quad y \equiv y - y_L; \quad z \equiv z - z_L,$$

$$\Phi_{xx} \equiv \left(\frac{\partial^2 \Phi_{\text{eff}}}{\partial x^2} \right)_{L_i}; \quad \Phi_{yy} \equiv \left(\frac{\partial^2 \Phi_{\text{eff}}}{\partial y^2} \right)_{L_i}; \quad \Phi_{zz} \equiv \left(\frac{\partial^2 \Phi_{\text{eff}}}{\partial z^2} \right)_{L_i}$$

and x_L , y_L and z_L are the coordinates of the Lagrangian point L_i . Note that, for any barlike potential whose principal axes lie along the coordinate axes, $\left(\frac{\partial^2 \Phi_{\text{eff}}}{\partial x \partial y} \right)_{L_i} = 0$ by symmetry. Setting $x_1 = x$, $x_2 = y$, $x_3 = z$, $x_4 = \dot{x}$, $x_5 = \dot{y}$ and $x_6 = \dot{z}$, equations (3) are written as a system of first order differential equations,

$$\begin{cases} \dot{x}_1 = f_1(x_1, \dots, x_6) = x_4 \\ \dot{x}_2 = f_2(x_1, \dots, x_6) = x_5 \\ \dot{x}_3 = f_3(x_1, \dots, x_6) = x_6 \\ \dot{x}_4 = f_4(x_1, \dots, x_6) = 2\Omega_p x_5 - \Phi_{xx} x_1 \\ \dot{x}_5 = f_5(x_1, \dots, x_6) = -2\Omega_p x_4 - \Phi_{yy} x_2 \\ \dot{x}_6 = f_6(x_1, \dots, x_6) = -\Phi_{zz} x_3. \end{cases} \quad (4)$$

² We can refer to Pfenniger (1990), where he studied the stability character of the Lagrangian points in different stellar bars.

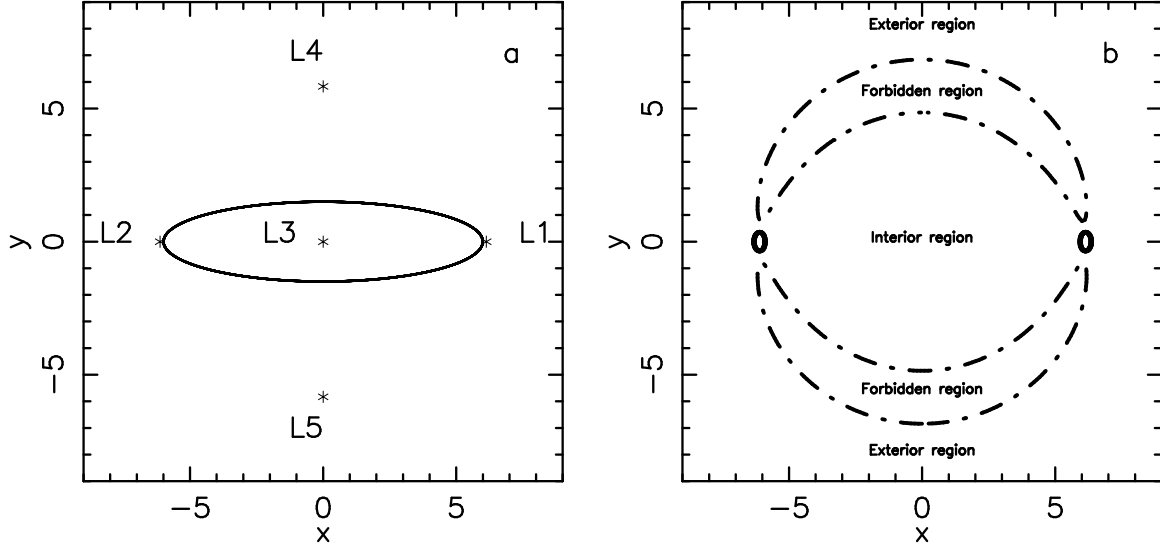


Fig. 2. a) Outline of the bar and the position of the five equilibrium points (marked with a star). **b)** The two Lyapunov orbits (thin solid lines) and the zero velocity curves (dot-dashed lines) delimiting the forbidden, the interior and exterior regions. Both are given for the same energy value.

3. Dynamics around L_1 . The invariant manifolds

3.1. Linear case

Let us now focus on the dynamics around L_1 (L_2 is completely symmetrical). The differential matrix associated to system (4) around L_1 is

$$Df_x(L_1) = \begin{pmatrix} 0 & 0 & 0 & 1 & 0 & 0 \\ 0 & 0 & 0 & 0 & 1 & 0 \\ 0 & 0 & 0 & 0 & 0 & 1 \\ -\Phi_{xx} & 0 & 0 & 0 & 2\Omega_p & 0 \\ 0 & -\Phi_{yy} & 0 & -2\Omega_p & 0 & 0 \\ 0 & 0 & -\Phi_{zz} & 0 & 0 & 0 \end{pmatrix}$$

We obtain the stability character of L_1 by studying the eigenvalues of this matrix. It has six eigenvalues: λ , $-\lambda$, ωi , $-\omega i$, νi and $-\nu i$, where λ , ω and ν are positive real numbers, i.e. L_1 is a linearly unstable point. The corresponding eigenvectors (either real or complex) have zero x_3 , and x_6 components in the case of $\pm\lambda$ and $\pm\omega i$, and zero x_1 , x_2 , x_4 , and x_5 components in the case of $\pm\nu i$. Since the purely imaginary eigenvalues denote oscillation and the real eigenvalues are associated to a saddle behaviour, i.e. exponential behaviour with opposite exponents, the linearised flow around L_1 in the rotating frame of coordinates is characterised by a superposition of an harmonic motion in the xy plane (equatorial plane), a saddle behaviour in this plane, and an oscillation in the z -direction.

Because of this unstable character, the equilibrium points L_1 and L_2 set the limits of the stability region around the stable point L_3 , and thus, they set an upper limit to the extension of the bar. This, however, is only an upper limit and in most cases the bar is much shorter than that limit (Athanasoula 1992; Patsis, Skokos & Athanasoula 2003).

The central stable point, L_3 , is surrounded by the classic x_1 family of periodic orbits which is responsible for maintaining the bar structure, while the stable points L_4 and L_5 are sur-

rounded by families of periodic banana orbits (Contopoulos & Papayannopoulos 1980; Athanasoula et al. 1983; Contopoulos 1981; Skokos, Patsis & Athanasoula 2002). All these orbits have been well studied for many models (Contopoulos 2002 and references therein) and we will not discuss them here any further.

As already mentioned, the general linear motion around L_1 is obtained by the addition of an hyperbolic exponential part to the in-plane and out-of-plane oscillations mentioned. We note that this exponential part has both stable and unstable components with exponents of opposite sign. Following again Binney & Tremaine (1987) we write

$$\begin{cases} x(t) = X_1 e^{\lambda t} + X_2 e^{-\lambda t} + X_3 \cos(\omega t + \phi), \\ y(t) = X_4 e^{\lambda t} + X_5 e^{-\lambda t} + X_6 \sin(\omega t + \phi), \\ z(t) = X_7 \cos(\nu t + \psi). \end{cases} \quad (5)$$

Here X_i , $i = 1, \dots, 7$ and ϕ , ψ are values representing amplitudes and phases. Substituting these equations into the differential equations (3), we find that X_i are related by

$$\begin{aligned} X_4 &= \frac{\Phi_{xx} + \lambda^2}{2\Omega_p \lambda} X_1 = -\frac{2\Omega_p \lambda}{\Phi_{yy} + \lambda^2} X_1 \\ X_5 &= -\frac{\Phi_{xx} + \lambda^2}{2\Omega_p \lambda} X_2 = \frac{2\Omega_p \lambda}{\Phi_{yy} + \lambda^2} X_2 \\ X_6 &= \frac{\Phi_{xx} - \omega^2}{2\Omega_p \omega} X_3 = \frac{2\Omega_p \omega}{\Phi_{yy} - \omega^2} X_3 \end{aligned} \quad (6)$$

We define $A_1 = \frac{\Phi_{xx} + \lambda^2}{2\Omega_p \lambda}$ and $A_2 = \frac{\Phi_{xx} - \omega^2}{2\Omega_p \omega}$. Note that A_1 depends only on λ and A_2 depends only on ω . Moreover $X_4 = A_1 X_1$, $X_5 = -A_1 X_2$, and $X_6 = A_2 X_3$, so that equation (5) becomes

$$\begin{cases} x(t) = X_1 e^{\lambda t} + X_2 e^{-\lambda t} + X_3 \cos(\omega t + \phi), \\ y(t) = A_1 X_1 e^{\lambda t} - A_1 X_2 e^{-\lambda t} + A_2 X_3 \sin(\omega t + \phi), \\ z(t) = X_7 \cos(\nu t + \psi). \end{cases} \quad (7)$$

In the sequel we will restrict ourselves to the motion in the equatorial plane (i.e. $z = 0$, or $X_7 = 0$). This restriction is not critical in the dynamics we want to study, since the z component essentially only adds a vertical oscillation to the planar motion. For a study of the vertical orbital structure around the Lagrangian points in barred galaxies, see Ollé & Pfenniger (1998).

Using (7), a given state (x, y, \dot{x}, \dot{y}) at $t = 0$ is characterised by a choice of (X_1, X_2, X_3, ϕ_1) , modulus 2π in the phase ϕ . When $X_1 = X_2 = 0$ the initial condition is of the form

$$(x(0), y(0), \dot{x}(0), \dot{y}(0)) = (X_3 \cos \phi, A_2 X_3 \sin \phi, -X_3 \omega \sin \phi, A_2 X_3 \omega \cos \phi)$$

for selected values of X_3 and ϕ . When time evolves, we obtain from this initial condition the periodic motion,

$$\mathbf{x}_0(t) = (x, y, \dot{x}, \dot{y}) = (X_3 \cos(\omega t + \phi), A_2 X_3 \sin(\omega t + \phi), -X_3 \omega \sin(\omega t + \phi), A_2 X_3 \omega \cos(\omega t + \phi)),$$

of period τ to which we will refer as a linear Lyapunov periodic orbit.

Consider now any small deviation δ from the periodic orbit $\mathbf{x}_0(t)$, $\mathbf{x}(t) = \mathbf{x}_0(t) + \delta$. Inserting this into the equations of motion (4), and linearising them with respect to δ , we obtain the variational equations

$$\dot{\delta} = \frac{\partial \mathbf{f}}{\partial \mathbf{x}} \delta = \sum_{i=1}^6 \left(\frac{\partial f_k}{\partial x_i} \right)_{\mathbf{x}_0} \delta_i \quad (8)$$

as defined in Contopoulos (2002), where

$$A(t) = (\delta_{ik}) = \left(\frac{\partial f_k}{\partial x_i} \right) = \begin{pmatrix} \frac{\partial f_1}{\partial x_1} & \dots & \frac{\partial f_1}{\partial x_6} \\ \vdots & \ddots & \vdots \\ \frac{\partial f_6}{\partial x_1} & \dots & \frac{\partial f_6}{\partial x_6} \end{pmatrix}$$

is the variational matrix. The variational equations are linear equations in δ_i ($i = 1, \dots, 6$) with periodic coefficients of period τ . These equations are used to study the stability character of a periodic orbit. If we integrate the variational equations (8) until time τ with initial conditions $\delta_{1k} = (1, 0, \dots, 0), \dots, \delta_{6k} = (0, \dots, 0, 1)$, we obtain the monodromy matrix. The eigenvalues and eigenvectors of the monodromy matrix give us information on the stability character of a periodic orbit.

Returning to equations (7), let us consider a similar initial condition but with $X_1 = 0$ and $X_2 \neq 0$. According to (7) the exponential term proportional to X_2 vanishes when time tends to infinity and the trajectory tends to the linear Lyapunov. All these type of orbits form what is called the stable manifold of the linear Lyapunov. In the same way, if the initial condition is chosen with $X_1 \neq 0$, $X_2 = 0$ the exponential term proportional to X_1 tends to zero when time tends to minus infinity, and all such orbits form what is called the unstable manifold of the linear Lyapunov. Roughly speaking, orbits in the stable/unstable manifold are asymptotic orbits, which tend to/depart from the linear Lyapunov orbit.

Initial

Condition on Unstable Invariant Manifold $(\phi, 0)$

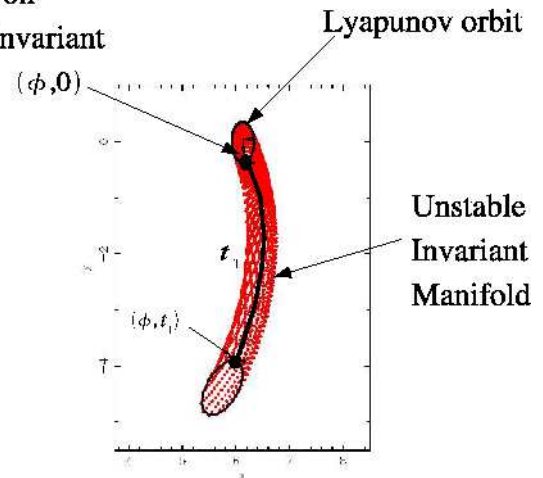


Fig. 3. Schematic view of an unstable invariant manifold.

3.2. General case

All the definitions given in section 3.1 for the linear case are easy to extend to the general case when the full equations of motion are considered. From L_1 emanates a family of planar periodic orbits known as Lyapunov orbits (Lyapunov 1949) which locally can be parametrised by the energy. The full set of Lyapunov orbits form a family of periodic orbits, which we will denote by Γ .

Let us denote by $\Psi(t, X)$ the orbit that at $t = 0$ has the state $X = (x, y, \dot{x}, \dot{y})$. For a given $\gamma \in \Gamma$, i.e. for a given Lyapunov orbit, we define the stable manifold of γ as

$$W_\gamma^s = \left\{ X \in \mathbb{R}^4 \ / \ \lim_{t \rightarrow \infty} \|\Psi(t, X) - \gamma\| = 0 \right\},$$

where the double bars denote Euclidean distance. Thus, simply speaking, the stable manifold is the set of orbits which tend to the Lyapunov orbit as time tends to infinity. In the same way, the unstable manifold of γ is defined as

$$W_\gamma^u = \left\{ X \in \mathbb{R}^4 \ / \ \lim_{t \rightarrow -\infty} \|\Psi(t, X) - \gamma\| = 0 \right\}.$$

Simply speaking again, the unstable manifold is the set of orbits which tend to the Lyapunov orbit as time tends to minus infinity, or, equivalently, the set of orbits departing from the Lyapunov. The orbits of W_γ^s and W_γ^u have the same energy as the Lyapunov orbit γ , and so they belong to the same energetic three dimensional manifold where γ is contained. Moreover, W_γ^s and W_γ^u are two dimensional tubes, which, similarly to the former linear example, can be parametrised by the angle ϕ and the time t (see Fig. 3 and Masdemont (2005)). We also note that both W_γ^s and W_γ^u have two branches meeting at the Lyapunov orbit in a way similar to a saddle point (see Fig. 4).

4. The role of invariant manifolds

Invariant manifolds of Lyapunov orbits play a crucial role in the transport of material between different parts of the configuration space. Lyapunov orbits are located near the ends of the

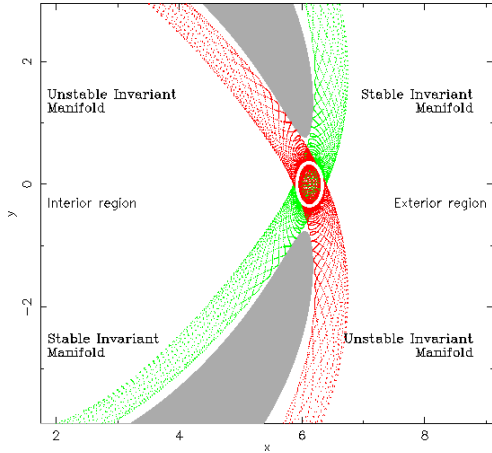


Fig. 4. Invariant manifolds. In the centre of the plot, and in white solid line, the Lyapunov orbit around L_1 . The two branches of the unstable invariant manifold (red or dotted lines), and the two branches of the stable invariant manifold (green or dotted lines). In grey, the forbidden region surrounded by the zero velocity curves.

bar of the galaxy, between the two banana like zero velocity curves which surround the forbidden regions of motion for the considered energy, and, loosely speaking, can be considered as gates between the interior and exterior region they delimit (see Fig 2b). Let us consider for instance the stable manifold, W_γ^s , inside the interior region and integrated backwards in time till it crosses the plane, S , defined by $x = 0$. The plot of this intersection in the $y\dot{y}$ plane is a closed curve $W_{\gamma,1}^s$ (Fig. 5). Each point in the plane $y\dot{y}$ of S corresponds to a given trajectory, since $x = 0$ by the definition of S and \dot{x} can be obtained from the condition that the energy of the state (x, y, \dot{x}, \dot{y}) be the selected one (the sign of \dot{x} is determined by the sense of crossing). $W_{\gamma,1}^s$ is a closed curve that splits the $y\dot{y}$ plane in S in three different regions: the curve itself, the points exterior to the curve and the points interior to the curve. By definition, the points on the curve $W_{\gamma,1}^s$ belong to W_γ^s and are therefore orbits that tend asymptotically to the Lyapunov orbit. The points outside $W_{\gamma,1}^s$ are states whose trajectories remain inside the interior region of the galaxy delimited by the zero velocity curves, while the points inside $W_{\gamma,1}^s$ correspond to orbits that transit from the interior region to the exterior one. These last orbits, the transit orbits, are confined inside the tube W_γ^u and, as we will argue in the following sections, are the orbits which form part of the rings of the galaxy for the considered energy value. In this way, the manifolds of the Lyapunov orbits drive the motion of the stars from the interior to the exterior regions. For more details of this mechanism, although in another context, see Gómez et al. (2004) and references therein. Since these invariant manifolds are not limited to the vicinity of the unstable points, but extend well beyond it, they can be responsible for global structures and we will argue in this paper that they, together with the orbits driven by them, could be responsible for the ring structures in barred galaxies.

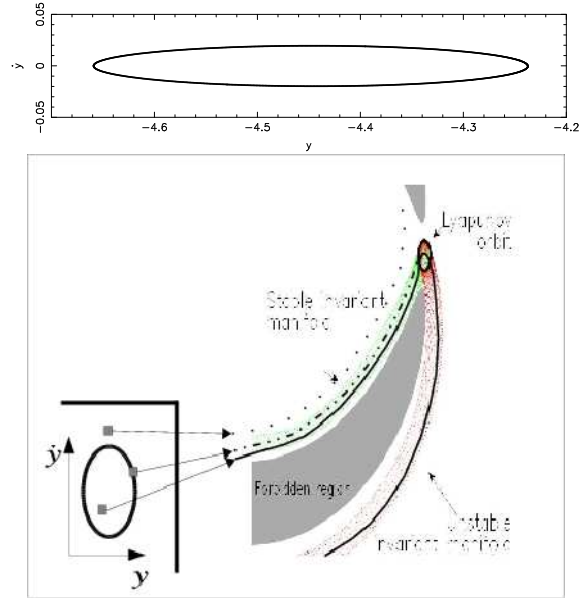


Fig. 5. Transport of material. **Top panel:** the curve $W_{\gamma,1}^s$ in the $y\dot{y}$ plane. **Bottom panel:** schematic view of the dynamics in the region around the L_1 Lagrangian point. In grey, the region delimited by the zero velocity curves. The dotted line gives a non-transit orbit, which is confined to the interior region and whose intersection with the $y\dot{y}$ plane is located outside the $W_{\gamma,1}^s$ curve; the solid line, a transit orbit, which in the $y\dot{y}$ plane is located inside the $W_{\gamma,1}^s$ curve; and the dot-dot-dash line, an asymptotic orbit of the stable invariant manifold. In the inlay, a schematic view of the curve $W_{\gamma,1}^s$ in the $y\dot{y}$ plane with the location of the three orbits.

5. Application to a ringed barred galaxy model

In this section we will explicitly calculate the invariant manifolds in a barred galaxy model. The reader who has only skimmed the previous sections should keep in mind that the invariant manifolds are just ensembles of orbits linked to the L_1 and L_2 Lyapunov orbits.

Since invariant manifolds can only be calculated numerically, we first adopt a simple, yet realistic, barred galaxy model (Pfenniger 1984). Our model bar consists of an axisymmetric component, modelled by a Miyamoto-Nagai potential (Miyamoto & Nagai 1975)

$$\Phi_d = - \frac{GM_d}{\sqrt{x^2 + y^2 + (A + \sqrt{B^2 + z^2})^2}},$$

and a Ferrers bar (Ferrers 1877)

$$\rho = \begin{cases} \rho_c(1 - m^2)^n & m \leq 1 \\ 0 & m \geq 1, \end{cases}$$

where $m^2 = x^2/a^2 + y^2/b^2 + z^2/c^2$ and $\rho_c = \frac{105}{32\pi} \frac{GM_b}{abc}$ is the central density. We take $A = 3$, $B = 1$, $n = 2$, $a = 6$, $b = 1.5$, $c = 0.6$, $GM_d = 0.9$ and $GM_b = 0.1$. The pattern speed is taken such as to place corotation at the end of the bar. The length unit is the kpc , the total mass $G(M_d + M_b)$ is set to be equal to

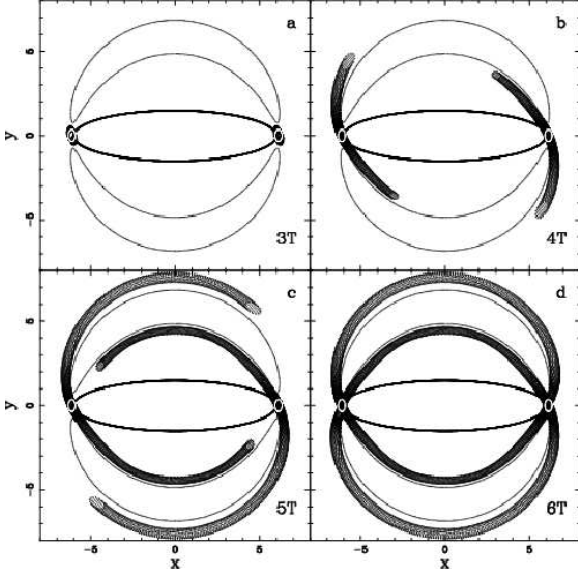


Fig. 6. Unstable invariant manifolds for four different times given in the lower right corner of each panel. T is the period of the bar rotation.

1, and the time unit is 2×10^6 yr. With these units, the value of the potential energy at L_3 , $L_1(L_2)$, and $L_4(L_5)$ is -0.31503 , -0.19789 and -0.19456 , respectively. As done already in the previous sections, we limit ourselves to the $z = 0$ plane, since the instability we are interested in is contained to this plane and the z component only adds vertical oscillations, which are unimportant in this context.

In this model, we computed the invariant manifolds numerically using an approach similar to the one of Gómez et al. (1993), i.e. we use a linear approach to obtain the initial conditions of the orbits that constitute the invariant manifolds³. As previously mentioned, the linear motion around L_1 and L_2 consists of an hyperbolic exponential part in the in-plane and of an out-of-plane oscillation. The exponential part has both stable and unstable components, which correspond to the stable and unstable eigenvectors of the monodromy matrix of the Lyapunov orbits around L_1 and L_2 . Therefore, we obtain the initial conditions for the stable and unstable invariant manifolds shifting positions and velocities of the Lyapunov orbit by a small amount (10^{-5}) in the direction given by the stable and unstable eigenvectors, respectively. The global extension of the manifold is then obtained by integrating numerically with a Runge-Kutta-Fehlberg of orders 7-8.

Figure 6 shows the evolution of the length of the unstable invariant manifolds with time. Here, T is the rotation period of the bar. Since the invariant manifolds consist of a set of orbits, their time evolution is that of an orbit. So Fig. 6 shows the orbits composing the invariant manifolds integrated up to 3,4,5 and 6 bar rotations, respectively, in order to check their evolution with time. Note that they leave the vicinity of the Lyapunov orbits, and stay close to the zero velocity curves. When they get

to the $x = 0$ axis, they bend and head towards the opposite side of the bar, completing the ring structure. Thus our calculations show that the apocenter of the orbits is near the $x = 0$ axis. This is indeed where we would intuitively place them since the periodic orbits outside corotation are elongated perpendicular to the bar and since the zero velocity curves also reach their maximum distance from the center at $x = 0$. Also note that, although the Lyapunov orbit is unstable, the orbits in the manifold stay in its close vicinity for at least three bar rotations. By four bar rotation periods arm stubs are formed, while at five the arms have a winding of about $3\pi/4$. By six bar rotation periods the manifold has reached the opposite end of the bar. In other words, the growth is by no means linear, since growth is slow in the beginning and faster as time advances. Indeed, it takes more than three orbital periods to leave the vicinity of the Lyapunov orbit, the first half of the winding is developed in about $4.5T$ and the full winding in barely at $6T$. After $6T$, the orbits on the manifold are in the vicinity of the Lyapunov orbit. These orbits do not leave this region in another new direction, but they follow the direction given by the invariant manifolds already formed.

Relevant information for a value of the Jacobi constant ($E_J = -0.1977$) close to the one of the $L_1(L_2)$ equilibrium point, is given in Fig. 7. In all four panels, the bar is outlined by a black dot-dashed line, while the positions of the five Lagrangian points are marked with a star, and the dark grey lines correspond to the zero velocity curves of this particular value of E_J . This means that any orbit with this energy starting outside these curves cannot enter within them. We have also plotted the two plane unstable Lyapunov periodic orbits around the unstable Lagrangian points L_1 and L_2 (black solid lines). In Fig. 7a we show the unstable invariant manifolds for this value of E_J . Each of these manifolds is composed of two branches, an interior branch, lying in the interior region, and an exterior branch, lying in the exterior region. Each of these branches can be thought of as an ensemble of orbits moving away from the Lyapunov orbit. Both branches lie near the zero velocity curves and, as shown in Fig. 6, their length increases with time until they reach the opposite side of the bar from which they emanated. The interior branch, when complete, outlines well the loci of the inner rings in barred galaxies. The exterior branch, when complete, has a shape similar to that of the R_1 outer rings. From a dynamical point of view, in the phase space these branches are seen like tubes that drive the dynamics. In Fig. 7b we plot the stable invariant manifolds, for the same value of E_J . Again there are two branches, an interior and an exterior one. Note also that the space loci of the stable and unstable manifold is almost identical. There is, however, an important difference in that, for the stable manifold, the orbits filling these tubes will go *towards* the Lyapunov orbits, while for the unstable manifold they will go *away* from it. In Fig. 7c we show four sets of orbits starting from the vicinity of the Lyapunov orbits and following the four tubes that constitute the two branches of the unstable manifolds. This figure illustrates how the invariant manifolds drive the dynamics, since we can see that initial conditions in the vicinity of the Lyapunov orbit will follow, due to its unstable character, a trajectory close to the unstable invariant manifolds. In Fig. 7d, we represent the

³ Higher order approximations could be obtained using similar techniques as in Masdemont (2005), but with much more difficulty and regularity problems.

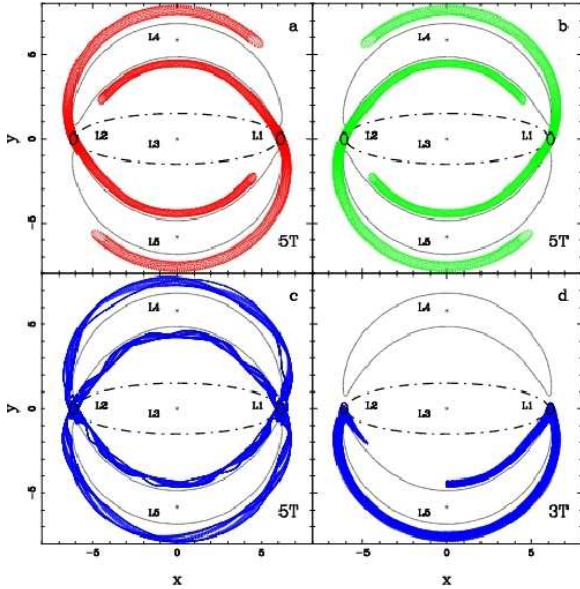


Fig. 7. Invariant manifolds and perturbations in the plane barred potential described in section 5 and for $E_J = -0.1977$. **a)** Invariant unstable manifolds coming from Lyapunov orbits around the Lagrangian points L_1 and L_2 . **b)** Invariant stable manifolds coming from the same Lyapunov orbits. **c)** Orbits starting from initial conditions near the Lyapunov orbit. **d)** Orbits starting from initial conditions inside the $W_{\gamma,1}^s$ curve of the interior branch of the stable invariant manifold.

trajectories with initial conditions inside the $W_{\gamma,1}^s$ curve of the interior branch of the stable invariant manifold, as explained in the previous section. This set of orbits follows the stable branch they emanate from, approaching the Lyapunov orbit, and it leaves the bar region following the exterior branch of the unstable invariant manifold.

6. Discussion

The time during which the orbit stays around the Lyapunov orbit before outlining the outer or the inner ring depends on the Lyapunov exponent (Lyapunov 1949) of the Lyapunov orbit, and is found to be an increasing function of E_J . Thus, orbits initially near the Lyapunov orbit with lower values of E_J stay less around the unstable point. This time increases gradually with the value of E_J , until the value at which the Lyapunov orbit becomes stable after which all orbits starting in the vicinity of the Lyapunov orbit stay around it. Thus the orbits outlining the rings are mainly low energy orbits. Repeating the computations in section 5 for different values of the Jacobi constant, $E_J = -0.1973$ and $E_J = -0.1960$, we find that the locus of the invariant manifolds (and therefore of the orbits associated to it) is roughly independent of their value of E_J . This is illustrated in Fig. 8b, for these two different values of E_J . As the energy increases, the size of the Lyapunov orbit also increases, so that the outline of the invariant manifold becomes thicker. However, as we consider more orbits and more energy levels, we find that the density of the central part of the outlined area increases considerably, so that in practice the thick-

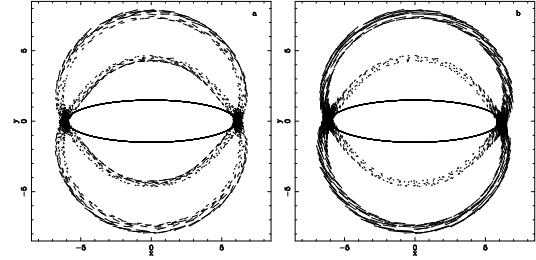


Fig. 9. Velocity field along the invariant manifolds. **a)** In the rotating frame. **b)** In the nonrotating frame.

ness of the ring will be considerably smaller than that of the higher energy manifolds. This is illustrated in Fig. 8a, where we plot the density profile on a cut across the ring. To obtain this figure we calculated the unstable invariant manifolds and the trajectories inside them for all energy levels at which the Lyapunov orbit is unstable, i.e. all energies for which the mechanism we propose can be applied. This covers the range of values from $E_J = -0.19789$, corresponding to the energy of the unstable equilibrium point, to the value $E_J = -0.1674$, where the Lyapunov family becomes stable. The contribution of each energy is weighted by a distribution function which is here simply assumed to be an exponentially decreasing function of the energy, i.e. of the form $\exp\left(-\frac{|E_J|}{2\sigma^2}\right)$, with $\sigma = 30\text{km s}^{-1}$ as a velocity dispersion characteristic of disc stars in the solar neighbourhood (Binney & Merryfield 1998). The exact shape of the distribution function is of little importance, but it has to be a decreasing function of the energies in the rotating frame of reference. The profile shown in Fig. 8a is very similar to those found for the old and intermediate age stellar population in rings and spirals (Schweizer 1976).

These ring structures will corotate with the bar. During bar evolution, however, the bar pattern speed will decrease with time due to an angular momentum exchange (Tremaine & Weinberg 1984; Weinberg 1985; Little & Carlberg 1991a, 1991b; Hernquist & Weinberg 1992; Athanassoula 1996; Debattista & Sellwod 2000; Athanassoula 2003; O’Neill & Dubinsky 2003; Valenzuela & Klypin 2003). This means that L_1 , L_2 , L_4 and L_5 will move outwards and thus the reservoir of fresh material for the rings would be continuously replenished. This may also be linked to the plumes that surround the ring structures of these galaxies (Buta 1984).

The model we propose here forms ring structures which are not necessarily associated with the outer Lindblad resonance. In fact, in the model shown in Fig. 7, the maximum radius of the inner branches of the invariants reaches values of about 4.25 radial units, while corotation radius is placed at the end of the bar at 6 radial units. The outer branches extend up to 7.5 radial units, while the Outer Lindblad Resonance of this model is placed at about 8.7 radial units. Note that the ratio of the maximum radius of the outer and inner branches give a value of 1.76 which is in agreement with the values of this ratio measured for ringed galaxies (Athanassoula et al. 1982; Buta 1995).

In the rotating frame, the velocities along the invariants reach a maximum at the point of maximum radius and then decrease toward the region of the Lyapunov orbits (see Fig. 9a).

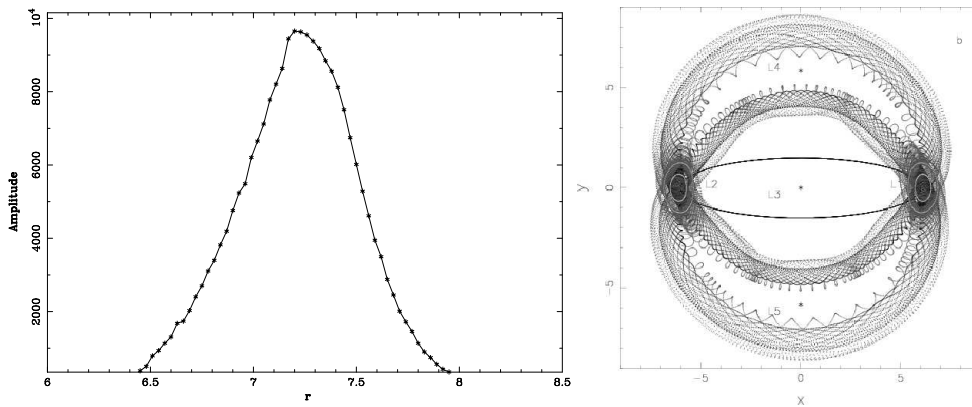


Fig. 8. a) Density profile on a cut across the ring. **b)** Two unstable invariant manifolds for different values of E_J . Note how similar the regions they delineate are.

In the non-rotating frame the velocities along the invariants are an order of magnitude higher in the outer branches than in the inner ones (see Fig. 9b). A clear prediction from our model is that the perturbations on the velocity fields produced by the rings should be higher around the outer ring than around the inner ring. There are little data available on the velocity fields along the rings of R_1 galaxies. The best data correspond to the galaxy NGC 1433 (Buta 1986b), which is of type R_1' . For this case, we can tentatively say that there is a general agreement with the oscillations in the velocities measured in the rotating frame for the inner ring.

Although these rings are not density waves, they do not have the shortcoming of material arms, since they do not wind up with time. A more appropriate name would be flux rings, since they are outlined by the trajectories of particles. The material of such rings would create a potential well. Other stars and gas in the galaxy would feel this potential and, while traversing the ring, they would stay longer at the potential minima, thus adding a density wave component to the ring. Thus, although we have not made any self consistent simulations, we can speculate that the flux rings and the density wave rings would coincide in the galaxy.

In this paper we presented a new theory on the origin of rR_1 ring structures based on orbital dynamics. We introduced the invariant manifolds of a periodic orbit, used so far in celestial mechanics. We explained their role in the transport of particles from the interior region to the exterior, and viceversa, and applied it to a realistic barred galaxy model. Finally, we compared and discussed our results and the characteristics of the rings obtained with observational data. We can conclude that the rR_1 ring structure can be interpreted as a bundle composed of all the invariant manifolds for all the possible energies as well as the orbits driven by them.

Acknowledgements We thank Albert Bosma for stimulating discussions on properties of observed rings. This work is being supported by the spanish MCyT BFM2003-9504 and catalan 2003XT-00021 grants. JJM also thanks the support of the Agrupació Astronòmica de Manresa.

References

- Athanassoula, E. 1992, MNRAS, 259, 328
 Athanassoula, E. 1996, Astron. Soc. Pac. Conf. Series, 91, 309
 Athanassoula, E. 2003, MNRAS, 341, 1179
 Athanassoula, E., Bienaymé, O., Martinet, L., Pfenniger, D. 1983, A&A, 127, 349
 Athanassoula, E., Bosma, A., Crézé, M., Schwarz, M.P. 1982, A&A, 107, 101
 Binney, J., Tremaine, S. 1987, Galactic Dynamics, Princeton Univ. Press, Princeton
 Binney, J., Merrifield, M. 1988, Galactic Astronomy, Princeton Univ. Press, Princeton
 Buta, R. 1984, Proc. Astron. Soc. Aus, 5, 472
 Buta, R. 1986a, ApJS, 61, 609
 Buta, R. 1986b, ApJS, 61, 631
 Buta, R. 1995, ApJS, 96, 39
 Buta, R., Alpert, A.J., Cobb, M.L., Crocker, D.A., Purcell, G.B., 1998, AJ, 116, 1142
 Contopoulos, G. 1981, A&A, 102, 265
 Contopoulos, G. 2002, Order and chaos in dynamical astronomy, Springer-Verlag, Berlin
 Contopoulos, G., Papayannopoulos, Th. 1980, A&A, 92, 33
 Danby, J.M.A. 1965, AJ, 70, 501
 Debattista, V.P., Sellwood, J.A. 2000, ApJ, 543, 704
 Ferrers N. M. 1877, Q.J. Pure Appl. Math., 14, 1
 Gómez G., Koon W.S., Lo M.W., Marsden J.E., Masdemont J.J., Ross S.D. 2004, Nonlinearity, 17, 1571
 Gómez, G., Jorba, A., Masdemont, J.J., Simó, C. 1993, Cel. Mech. and Dynam. Astron., 56, 239
 Hernquist, L., Weinberg, M.D. 1992, ApJ, 400, 80
 Little, B., Carlberg, R.G. 1991a, MNRAS, 250, 161
 Little, B., Carlberg, R.G. 1991b, MNRAS, 251, 227
 Lyapunov, A. 1949, Ann. Math. Studies, 17
 Masdemont, J.J. 2005, Dyn. Systems: an Int. Journ., 20, 59
 Miyamoto, M., Nagai, R. 1975, PASJ, 27, 533
 Ollé, M., Pfenniger, D. 1984, A&A, 334, 829
 O'Neill, J.K., Dubinski, J. 2003, MNRAS, 346, 251
 Patsis, P.A., Skokos, Ch., Athanassoula, E. 2003, MNRAS, 342, 69
 Pfenniger, D. 1984, A&A, 134, 373
 Pfenniger, D. 1990, A&A, 230, 55
 Schwarz, M.P. 1981, ApJ, 247, 77
 Schwarz, M.P. 1984, MNRAS, 209, 93
 Schwarz, M.P. 1985, MNRAS, 212, 677
 Schweizer, F., 1976, ApJS, 31, 313
 Skokos, Ch., Patsis, P.A., Athanassoula, E. 2002, MNRAS, 333, 874.

- Tremaine, S., Weinberg, M.D. 1984, MNRAS, 209, 729
Valenzuela, O., Klypin, A. 2003, MNRAS, 345, 406
Weinberg, M.D. 1985, MNRAS, 213, 451